Draft version May 26, 2023
Typeset using LaTeX **twocolumn** style in AASTeX631

L Band Phased Array Feed Noise Figure and Radiation Efficiency Measurement with the Antenna Y Factor Method

Mitchell C. Burnett,[1] David Buck,[1] Nathaniel Ashcraft,[1] Spencer Ammermon,[1] Brian D. Jeffs,[1] and Karl F. Warnick[1]

[1] *Department of Electrical And Computer Engineering, Brigham Young University, Provo, UT 84602, USA*

ABSTRACT

The noise performance of a high sensitivity, wide-field astronomical phased array feed receiver can be characterized by measurements using the antenna Y factor method. These measurements are used to determine figures of merit for an active array receiver. Antenna elements for the Advanced L Band Phased Array Camera for Astronomy (ALPACA) were measured using the antenna Y factor method to determine the active array and receiver noise figure, the antenna loss, receiver equivalent noise temperature, and radiation efficiency of the system over its 500 MHz operating bandwidth. The completed ALPACA instrument will feature a fully cryogenic design with both the low-noise amplifiers and array elements cryogenically cooled. The uncooled performance measurements from the antenna Y factor method are used to extrapolate the elements cryogenic radiation efficiency and antenna loss showing that it is expected that the elements will contribute less than 1 K to the overall system noise temperature. These results validate the antenna Y factor method to measure key antenna parameters such as the antenna radiation efficiency and show that the instruments front end array and electronics meets expected performance targets.

1. INTRODUCTION

Receiver systems for applications in radio astronomy, satellite communications, radar, and remote sensing require high antenna efficiency. Radiation losses in the antenna elements exact a double penalty on SNR by reducing the received signal power and increasing thermal noise. When diagnosing and optimizing the design of high-sensitivity receivers, methods are needed to accurately quantify antenna radiation efficiency.

For a highly efficient antenna, measuring or simulating its radiation efficiency is challenging. Most methods require expensive equipment or are difficult to use for large array systems. Radiation efficiency can be measured with the Wheeler cap method (Pozar & Kaufman 1988), but computing the radiation efficiency requires the choice of an antenna circuit model and the conducting cavity used in the method can perturb the current distribution on the antenna. A well-calibrated antenna range can also be used to determine gain and directivity and infer the radiation efficiency (Yang et al. 2013; Senic et al. 2017), but this is a costly measurement procedure that is hard to apply to large systems. Numerical modeling of radiation efficiency requires subtracting integrated radiated power from the input power at the antenna port, and commercial modeling software packages are in general not accurate enough to model the radiation losses in highly efficient antennas. Due to numerical error, radiated power can be higher than input power, which violates conservation of energy. Specialized numerical techniques have been used successfully to determine the efficiency of low-loss antennas (Maaskant et al. 2009).

Another technique for experimentally quantifying the performance of a high-sensitivity receiver is the antenna Y factor method. The antenna Y factor method—founded upon the principles of the benchtop Y factor measurement for characterizing microwave systems—measures the noise response of the antenna and connected receiver electronics in the active antenna system (Ashkenazy et al. 1985; Woestenburg & Dijkstra 2003; Warnick et al. 2009; Beaulieu et al. 2016; Warnick 2017). The receiver system may consist of a single antenna or a large, complex antenna array with digitally formed beams. The antenna Y factor method in its basic form determines the noise performance of the full receiver system, including noise due to losses in the antenna and noise added by the receiver electronics after the antenna

Corresponding author: Mitchell C. Burnett
mitch.burnett@byu.edu

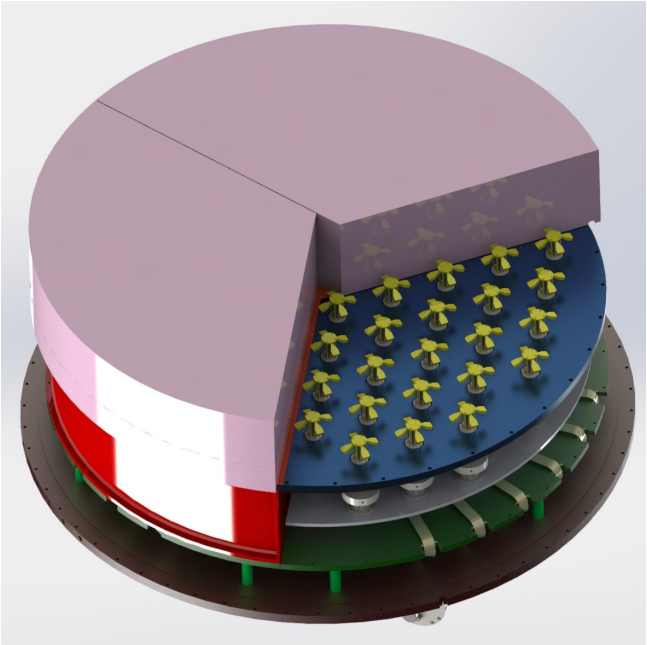

Figure 1. Viewing the ALPACA cryostat with the vacuum window and one section of the RF clear foam removed. The dipole array is shown along with components of the cryostat: ground plane (blue), radiation shield (red), 25 K base plate (gray), and 80 K base plate (green).

in the signal chain. This is parameterized by the active antenna noise figure (Warnick 2022). The antenna Y factor technique has been included in the latest revision of the IEEE Recommended Practice for Antenna Measurements, Std 149-2021 (2022).

The basic antenna Y factor method gives the noise figure of the antenna and receiver as a combined system, but with additional information, noise due to antenna losses can be separated from the receiver noise and the antenna radiation efficiency determined. This can be done with a well-characterized front end amplifier or a reference antenna with an efficiency close to unity (Ashkenazy et al. 1985; Pozar & Kaufman 1988). In this paper, we use a separate measurement of the equivalent noise temperature of the front end receiver electronics following the antenna. With an accurate measurement of the receiver noise, the radiation efficiency of the antenna under test can be determined from the antenna Y factor measurement.

This method for measuring the active noise figure and the antenna radiation efficiency was used to characterize the front end of the advanced L band phased array camera for astronomy (ALPACA) (Burnett et al. 2020). Figure 1 shows a rendering of the ALPACA cryostat with part of the vacuum window and RF clear foam removed showing the array elements. This instrument will be a fully cryogenic wide-field 69-element phased array feed and digital beamformer back end. Array elements are a dual-polarized broadband dipole that have been geometrically optimized to maximize beamformed array sensitivity (Warnick et al. 2019).

For the antenna Y factor measurement, an ALPACA dipole was placed in a copper ground shield to block ground noise. The hot load was microwave absorber foam and the cold load was the microwave sky. The Y factor was measured over the ALPACA L band operating frequency range. The dipole was connected to an uncooled LNA and additional gain blocks and the noise power measured with a spectrum analyzer. The noise figure of the LNA and gain blocks was measured using a connectorized microwave noise source. These measured values were used to estimate the antenna radiation efficiency. The ambient temperature measurements were extrapolated to estimate the noise temperature contribution of the dipole element at cryogenic temperatures. These results help to validate the extension of the antenna Y factor method to measure antenna radiation efficiency and provide a characterization for the expected performance of the ALPACA receiver.

2. ANTENNA Y FACTOR MEASUREMENT TECHNIQUE

In the antenna Y factor method, a hot thermal noise distribution and a cold noise distribution external to the antenna are used to probe the properties of an antenna and receiver system (Warnick et al. 2009; Chippendale et al. 2014). The Y factor is the ratio of the noise powers at the system output with the hot and cold loads. From the Y factor, the equivalent active antenna temperature can be computed using (Kerr 1999)

$$T_{\rm eq} = \frac{T_{\rm hot} - Y T_{\rm cold}}{Y - 1}, \tag{1}$$

where $T_{\rm hot}$ and $T_{\rm cold}$ are the brightness temperatures of the hot and cold external noise distributions.

Microwave absorber at ambient temperature is commonly used as the hot load. The cold load is the microwave sky with a ground shield to block thermal radiation from warm ground and objects near the horizon. For the antenna parameters computed from the antenna Y factor method to agree with IEEE standard definitions for antenna terms, the temperature distributions of the hot and cold loads must be isotropic. If ground noise scatters into the antenna field of view a correction can be made to $T_{\rm cold}$ to adjust for the small anisotropy in the cold load temperature distribution (IEEE Std 149-2021 2022).

2.1. *Active antenna noise figure*

A definition for the noise figure of an active antenna system is given in (Warnick 2022). Using the relationship $F = 1 + T_{\rm eq}/T_0$, the active antenna noise figure can be found from the Y factor using

$$F = \frac{T_{\rm hot} - T_0 + Y(T_0 - T_{\rm cold})}{(Y-1)T_0}. \quad (2)$$

This is the noise figure of the antenna and receiver. It parameterizes the noise performance of the system including the antenna and all amplifiers, transmission lines, and electronics in the signal chain from the antenna port to the system output. The active antenna noise figure captures all contributions to the system noise except for noise from sources external to the antenna. By convention, the external thermal environment is isotropic when measuring the active antenna noise figure.

2.2. *Antenna Y factor method and the system noise budget*

We now consider how the equivalent temperature in (1) relates to the system noise budget. The system noise temperature is

$$T_{\rm sys} = T'_{\rm ext} + T_{\rm loss} + T_{\rm rec}. \quad (3)$$

The external noise contribution is $T'_{\rm ext} = \eta_{\rm rad} T_{\rm ext}$, where $T_{\rm ext}$ is the temperature of the noise environment around the antenna and $\eta_{\rm rad}$ is the antenna radiation efficiency. For antenna array receiver systems that include nonreciprocal components, the radiation efficiency is replaced by the receiving efficiency (IEEE Std 145-2013 2014). $T_{\rm rec}$ is the equivalent receiver noise temperature associated with amplifiers and electronic components after the antenna. The noise due to antenna losses is

$$T_{\rm loss} = (1 - \eta_{\rm rad}) T_{\rm p}, \quad (4)$$

where $T_{\rm p}$ is the physical temperature of the antenna. For the measurements reported in this paper, the antenna physical temperature is the ambient outdoor temperature. In operation, the ALPACA receiver array is within a cryostat under a vacuum window and the maximum expected physical temperature of the dipoles is 25 K.

By convention the system noise temperature (3) is referred to the antenna terminals after antenna losses. If we move the reference plane before antenna losses (i.e., to an equivalent sky temperature), we obtain

$$\frac{T_{\rm sys}}{\eta_{\rm rad}} = T_{\rm ext} + \underbrace{\frac{T_{\rm loss} + T_{\rm rec}}{\eta_{\rm rad}}}_{T_{\rm eq}}. \quad (5)$$

It can be shown that the second term on the right hand side is the equivalent temperature (1) measured by the antenna Y factor method (Warnick 2022; Kerr 1999). The antenna Y factor method therefore determines the antenna loss and receiver noise contribution to the overall system noise budget at a reference plane before antenna losses.

2.3. *Measuring radiation efficiency*

The antenna Y factor method measures the combined noise performance of the antenna and receiver system. This was shown in (5) to be an equivalent temperature for the active antenna. However, the antenna and receiver noise contributions are together increased by the antenna radiation efficiency. Their individual contributions cannot be determined without additional information.

Equating the equivalent temperature for the antenna Y factor as in (1) and using (4) for the antenna loss noise, the antenna radiation efficiency in terms of the antenna Y factor and receiver noise temperature is (Warnick 2022)

$$\eta_{\rm rad} = \frac{(T_{\rm p} + T_{\rm rec})(Y-1)}{T_{\rm hot} - T_{\rm p} + Y(T_{\rm p} - T_{\rm cold})}, \quad (6)$$

where $T_{\rm p}$ is again the physical antenna temperature and $T_{\rm hot}$ and $T_{\rm cold}$ are the brightness temperatures of the hot and cold external noise distributions when measuring Y for the antenna Y factor. When the physical antenna temperature and hot load can be approximately considered to be at the same temperature (6) can be simplified and reduces to

$$\eta_{\rm rad} = \frac{(T_{\rm p} + T_{\rm rec})(Y-1)}{Y(T_{\rm p} - T_{\rm cold})}. \quad (7)$$

The relative sensitivity of the radiation efficiency to variations in the cold sky temperature $T_{\rm cold}$ is proportional to $\Delta T_{\rm cold}/T_{\rm hot}$. For typical L band sky temperatures, uncertainty in the cold sky temperature translates to a relative error of ± 0.01 in the measured radiation efficiency, which is relatively low and smaller than the typical uncertainty in the Y factor measurement.

To measure the radiation efficiency and subsequently determine the separate noise contributions an additional measurement to compute the receiver noise temperature is needed. The measurement of $T_{\rm rec}$ is made using the standard benchtop Y factor method as previously discussed. This process of obtaining a secondary measurement of the receiver noise temperature to be used jointly with the antenna Y factor can be considered an extensions of the antenna Y factor method for determining the antenna radiation efficiency.

3. EXPERIMENTAL RESULTS

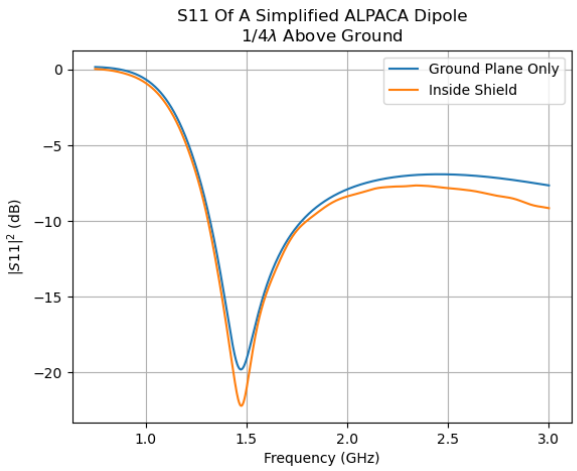

Figure 2. Comparison of simulated S-parameters for a simple dipole model above a ground plane only and inside a ground shield. The presence of the ground shield has minimal influence on antenna matching, indicating the ground shield is not strongly coupled to the antenna and will not perturb the antenna radiation efficiency measurement.

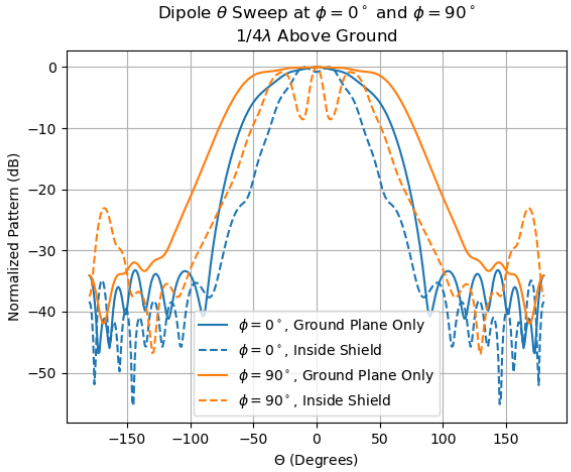

Figure 3. Simulation comparing radiation patterns of a simple dipole model using a ground plane only and the same dipole within the proposed ground shield geometry. The ground shield reduces the main beamwidth of the antenna radiation pattern and blocks thermal contributions from ground sources in the Y factor measurement.

The antenna Y factor and radiation efficiency measurement technique of the previous section were used to characterize the ALPACA L band dipole antenna element. The experiment was conducted at a remote outdoor location to provide an environment with as little in-band radio interference as possible.

A custom copper screen ground shield was constructed. The geometry of the ground shield was designed using a simplified dipole model and finite-difference time-domain electromagnetic field solver (Empire XPU). The design goal was to block thermal radiation from the ground while minimizing the impact of the ground shield on the antenna radiation pattern. S-parameters and radiated field patterns for these simulations are depicted in Figures 2 and 3, respectively. The influence of the shield on the dipole S-parameters was negligible. The main lobe of the radiation pattern is perturbed by the ground shield. In view of the near isotropic distribution of the hot and cold thermal loads, the effect of the pattern perturbations is negligible.

The Y factor measurements were made using the ALPACA instrument receiver and signal transport links. For a single polarization of an array dipole, a flexible stripline carried the LNA output signal from the antenna and coupled it to a low-noise RF-over-fiber (RFoF) link for long-haul transport to the digital beamformer back end (Burnett et al. 2022). A full transport link with a 2 km spool of optical fiber was used. The RFoF downlink was connected to a ZCU216 RF-system-on-chip (RFSoC) direct sampling at L band with an instantaneous bandwidth of 500 MHz centered at 1500 MHz. ADC output samples were channelized using a 1024-point FFT with power averaging over 64K frames to reduce sample estimation error in the hot and cold power measurements.

Figures 4 and 5 show the experiment setup at the remote site and the wood-framed stand with conductive ground shield to support the antenna under test. The base of the shield had a copper ground plane below a rectangular funnel with 16 mesh copper walls. Antenna Y factor measurements were made after sunset with the opening of the shield pointed up to the sky for cold Y factor measurements. When making hot measurements, a large rigid panel with microwave absorber was placed over the opening of the shield making contact with the inner walls of the ground shield.

Measuring the radiation efficiency using (6) requires two separate Y factor measurements: one to calculate the equivalent noise temperature of the receiver, T_{rec}, and the other for the antenna and receiver system. Measurements of these quantities were made consecutively to reduce errors due to thermal drift over time. To enable this without disturbing the receiver equipment, the ground shield funnel was removable at the ground plane. This allowed the antenna to be disconnected from the receiver allowing access to the receiver input port for a calibrated noise source. The antenna and the hot load are the same outside ambient temperature and the radiation efficiency was computed using the simplified expression (7). Because the astronomical receiver is highly stable over a period of minutes, the receiver noise is the

Figure 4. Equipment at the remote measurement site with the conductive ground shield setup for a hot load antenna measurement for the Y factor method.

Figure 5. ALPACA dipole placed in the ground plane of the stand for the ground shield.

same in both the antenna and receiver Y factor measurement and the receiver Y factor measurement.

The receiver Y factor was measured using a connectorized noise source. The resulting equivalent receiver noise temperature computed from the receiver only measurement is shown in Figure 6. The antenna and receiver Y factor is shown in Figure 7. The antenna Y factor was used to compute the active antenna noise figure using (2) as shown in Figure 8.

As can be seen in the Y factor results, external noise and radio frequency interference (RFI) are a factor in the antenna measurement. It is challenging to measure the antenna Y factor at all frequencies in the band of interest due to interference from satellite services such as GPS and Iridium. In Figure 7, contributions from these interferes can be seen in the 1530-1630 MHz band. Despite the observed interference, the results show that it is practical to characterize the antenna performance

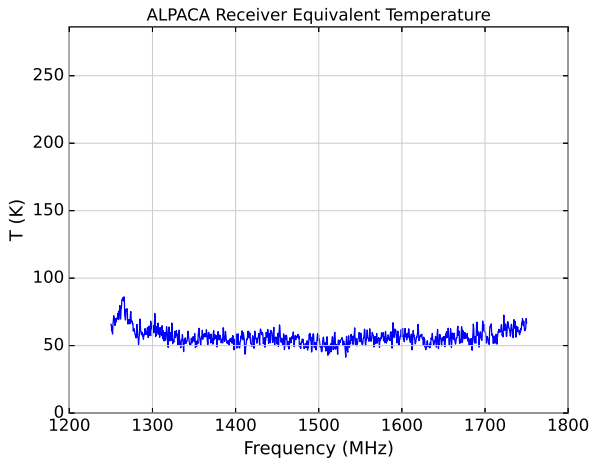

Figure 6. Equivalent receiver noise temperature computed from the receiver only Y factor for the ALPACA LNA and RFoF signal transport system measured with a connectorized noise source.

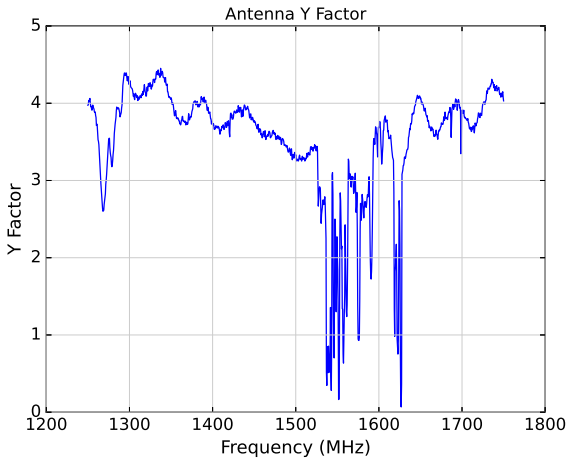

Figure 7. ALPACA dipole antenna and receiver Y factor showing the power ratio between the system output power with absorber foam (hot) and sky (cold) loads. The presence of satellite interferers can be seen in the band from 1530-1630 MHz.

over much of the ALPACA operating bandwidth. The receiver Y factor measurement is done using a fully connectorized setup and the effect of RFI is negligible in the receiver noise temperature results.

The measured radiation efficiency for the ALPACA dipole is shown in Figure 9. For this result, the physical antenna temperature, $T_{\rm p}$, was the outside ambient temperature, 283.15 K (50° F), and an estimate of the sky brightness temperature at L band, 6.88 K, was used for $T_{\rm cold}$. This estimate is based on a survey of measured sky brightness temperatures considering contributions from the cosmic microwave background, as well as con-

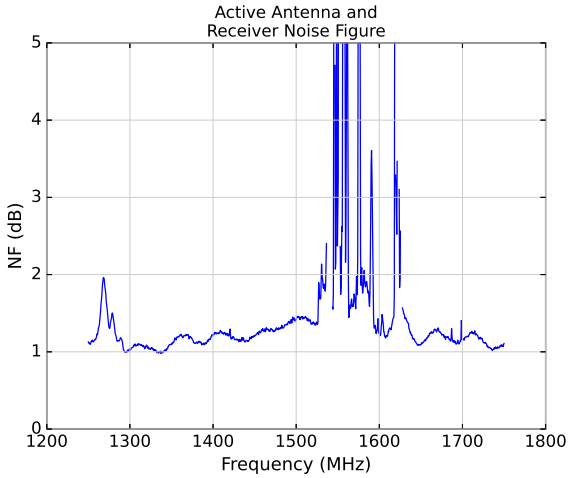

Figure 8. Measurement of the active antenna noise figure from the antenna Y factor method for an ALPACA dipole array element, LNA, and RFoF receiver link.

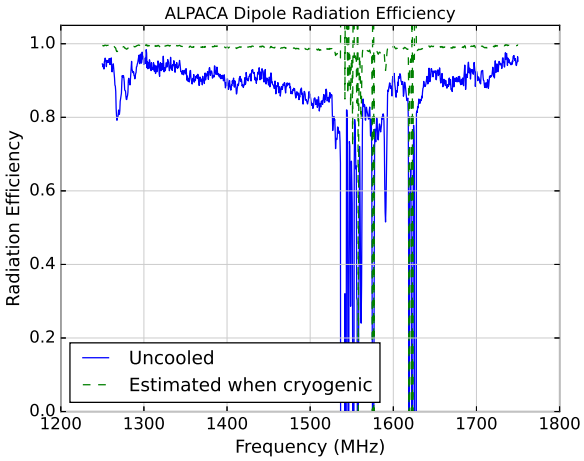

Figure 9. Measured radiation efficiency for a single polarization of an ALPACA dipole. Due to interference present in the Y factor measurement the efficiency is invalid for 1530-1630 MHz. The dipole has a radiation efficiency greater than 80% over its wide operating bandwidth.

tinuum and atomic hydrogen sources at declination 39° 45′ (Dinnat et al. 2018).

Ignoring frequencies corrupted by interference, over its wide operating bandwidth the ALPACA dipole has a measured radiation efficiency greater than 80%. With a measurement of the radiation efficiency for the dipole, contributions to the system equivalent noise temperature due to thermal losses in the antenna can be determined using $T_{\rm loss} = (1 - \eta_{\rm rad})T_{\rm p}$ as shown in Figure 10. The physical antenna temperature used here is the temperature used when measuring the antenna Y factor and calculating the radiation efficiency.

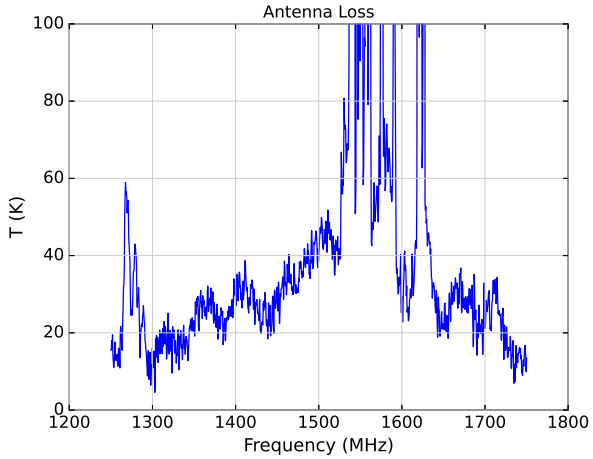

Figure 10. Thermal noise temperature contribution due to antenna losses for the uncooled ALPACA dipole using the previously computed radiation efficiency.

3.1. *Extrapolation to Cryogenic Temperatures*

In the completed instrument, the dipole and LNA will be cooled within the ALPACA cryostat. The goal of this measurement effort is to validate the ALPACA antenna element design and understand the impact of antenna losses on the receiver sensitivity. As the radiation efficiency measurements were made at ambient temperature, they must be extrapolated to cryogenic temperatures. This can be done using measured data for the electrical conductivity over temperature of the materials used in the antenna element.

The ALPACA dipole is fabricated primarily from Aluminum 6061. The coax core that runs from the wedge arms to SMA connector of the LNA is BeCU C17300. The entire dipole is 99.7% pure gold plated with minimum 100 micro-in (2.54 μm) thickness and a layer of copper for adhesion. At L band, the gold plating is several skin depths thick, so the gold substantially determines the electrical conductivity of the antennas.

At cryogenic temperatures, electrical conductivity is quantified by the relative resistivity ratio (RRR). This is the resistivity at room temperature relative to the resistivity near absolute zero temperature. The RRR is heavily dependent on the purity of the material, and consequently the conductivity of materials at cryogenic temperatures is complex and difficult to quantify precisely. The relationship between losses and and conductivity at microwave frequencies is further complicated by anomalous skin depth effects (Finger & Kerr 2008). Finger & Kerr (2008) give a value of 12 for the RRR of gold near the maximum expected ALPACA dipole operating temperature of 25 K. This was used to roughly estimate the dipole radiation efficiency when cooled.

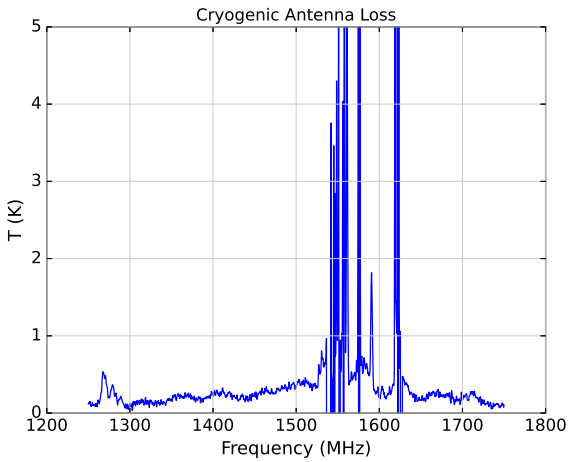

Figure 11. Estimated antenna loss contributions for the ALPACA dipole when operating inside the instruments cryostat at a temperature of 25 K.

Using a loss resistance model for the dipole, the radiation efficiency is

$$\eta_{\rm rad} = \frac{R_{\rm rad}}{R_{\rm rad} + R_{\rm loss}}, \tag{8}$$

where $R_{\rm rad}$ is the radiation resistance of the antenna element, and is nominally 50 Ω. With the measured radiation efficiency in Figure 9, the loss resistance, $R_{\rm loss}$, can be determined from (8). The loss resistance is reduced by the cryogenic RRR of the gold plating to estimate the radiation efficiency of the cooled antenna

$$\eta_{\rm rad,\ 20\,K} = \frac{R_{\rm rad}}{R_{\rm rad} + R_{\rm loss}/{\rm RRR}}. \tag{9}$$

This quantity is shown as the cryogenic radiation efficiency curve in Figure 9. Values for the predicted cryogenic antenna radiation efficiency that are greater than one correspond to RFI corrupted frequencies bands.

The estimated contribution of antenna losses to the ALPACA system noise budget computed from (4) using the cryogenic radiation efficiency is shown in Figure 11. The predicted value is below 1 K and is as expected based on the ALPACA system design targets. There is significant uncertainty in the RRR value for the materials used to fabricate the antenna elements. At the lowest possible value of the RRR, the predicted cryogenic antenna loss noise temperature in Figure 11 may be higher by 0.5 K, which remains within adequate performance ranges for the ALPACA receiver.

4. CONCLUSION

For sensitive astronomical phased array receivers, such as ALPACA, accurate yet simple techniques for characterizing the performance of a system are required. Existing methods such as direct measurements using a calibrated antenna range, or a numerical simulation using a high-quality loss model can be accurate. However, these methods can be costly and complex in their setup and implementation. With figures of merit for antenna and receiver systems defined in terms of measurable noise responses, the antenna Y factor method is a valuable technique for determining the noise response throughout the active receivers signal path. Measured results for the ALPACA L band array element and receiver signal chain validate the system design and shows that the extended Y factor method for measuring an antennas radiation efficiency is a practical approach for characterizing system losses due to the antenna element. Furthermore, with the unique ALPACA cryostat design for cooling the antenna elements, the extended Y factor method provides for an estimate of less than 1 K for the expected cryogenic system noise performance of the array elements. These results should allow the instrument to achieve required targets for system noise and sensitivity. In future work, it would be of interest to repeat the measurement for an array of antenna elements to assess the impact of coupling between elements on the measured radiation efficiency.

ACKNOWLEDGEMENT

This material is based upon work supported by National Science Foundation grant No. 1636645.

REFERENCES

2014, IEEE Std 145-2013 (Revision of IEEE Std 145-1993), 1, doi: 10.1109/IEEESTD.2014.6758443

2022, IEEE Std 149-2021 (Revision of IEEE Std 149-1977), 1, doi: 10.1109/IEEESTD.2022.9714428

Ashkenazy, J., Levine, E., & Treves, D. 1985, Electronics letters, 3, 111

Beaulieu, A. J., Belostotski, L., Burgess, T., Veidt, B., & Haslett, J. W. 2016, IEEE Antennas and Wireless Propagation Letters, 15, 1719

Burnett, M., Kunzler, J., Nygaard, E., et al. 2020, in 2020 XXXIIIrd General Assembly and Scientific Symposium of the International Union of Radio Science (URSI GASS), 1–4

Burnett, M. C., Ashcraft, N., Ammermon, S. M., Jeffs, B. D., & Warnick, K. F. 2022, in 2022 United States National Committee of URSI National Radio Science Meeting (USNC-URSI NRSM), 125–126, doi: 10.23919/USNC-URSINRSM57467.2022.9881396

Chippendale, A. P., Hayman, D. B., & Hay, S. 2014, Publications of the Astronomical Society of Australia, 31

Dinnat, E., Le Vine, D., Abraham, S., & N., F. 2018, Map of Sky Background Brightness Temperature at L-band, Recommendation, NASA Jet Propulsion Laboratory

Finger, R., & Kerr, A. 2008, International Journal of Infrared and Millimeter Waves, 29, 924

Kerr, A. R. 1999, IEEE transactions on microwave theory and techniques, 47, 325

Maaskant, R., Bekers, D. J., Arts, M. J., van Cappellen, W. A., & Ivashina, M. V. 2009, IEEE Antennas and Wireless Propagation Letters, 8, 1166

Pozar, D. M., & Kaufman, B. 1988, IEEE Transactions on Antennas and Propagation, 36, 136

Senic, D., Williams, D. F., Remley, K. A., et al. 2017, IEEE Transactions on Antennas and Propagation, 65, 4209

Warnick, K. F. 2017, in 2017 IEEE International Symposium on Antennas and Propagation & USNC/URSI National Radio Science Meeting, IEEE, 2059–2060

Warnick, K. F. 2022, Antennas and Wireless Propagation Letters, doi: 10.1109/LAWP.2022.3175146

Warnick, K. F., Jeffs, B. D., Landon, J., et al. 2009, in 2009 IEEE International Workshop on Antenna Technology, IEEE, 1–4

Warnick, K. F., Kunzler, J., & Cortes-Medellin, G. 2019, in 2019 IEEE International Symposium on Antennas and Propagation and USNC-URSI Radio Science Meeting, 399–400, doi: 10.1109/APUSNCURSINRSM.2019.8888810

Woestenburg, E., & Dijkstra, K. 2003, in 33rd European Microwave Conference Proceedings (IEEE Cat. No. 03EX723C), Vol. 1, IEEE, 363–366

Yang, Z., Warnick, K. F., & Holloway, C. L. 2013, in 2013 IEEE Antennas and Propagation Society International Symposium (APSURSI), IEEE, 1576–1577